RESEARCH ARTICLE

A unifying causal model of rate-independent linear damping for the effective seismic response reduction in low-frequency structures

Hao Luo[1] | Kohju Ikago*[2]

[1]School of Engineering, Tohoku University, Sendai 980-0845, Japan
[2]International Research Institute of Disaster Science, Tohoku University, Sendai 980-8572, Japan

Correspondence
*Kohju Ikago, International Research Institute of Disaster Science, Tohoku University, 468-1 Aramaki aza-aoba, Aoba, Sendai, Miyagi 980-8572, Japan.Email: ikago@irides.tohoku.ac.jp

Summary

It is well established that rate-independent linear damping (RILD) yields similar performance in controlling seismic response displacement to that of linear viscous damping having the same loss factor when incorporated into a structure, whereas the damping force generated by RILD is relatively low in the frequency range that is higher than the natural frequency of the primary structure. This leads to efficient displacement control with low damping force and floor response acceleration when RILD is incorporated into low-frequency structures. However, the non-causality of RILD hinders its practical applications, and thus causal models to mimic the behavior of RILD are pursued by many researchers.
This paper proposes a novel causal model of RILD using Maxwell elements whose damping force is generated according to the fractional-order derivative of displacement. The proposed model also represented by a fractional-order filter is found to be a unifying model that encompasses known causal RILD models developed by independent researchers, bringing insights to the nature of RILD.
Moreover, several methods to physically realize the proposed model are examined.

KEYWORDS:
Rate-independent linear damping, Maxwell model, fractional-order derivative, low-frequency structure.

1 | INTRODUCTION

Rate-independent linear damping (RILD) is found to benefit low-frequency structures by effectively reducing excessive seismic response displacements without increasing floor response accelerations when subjected to strong ground motions [1,2]. The aim of this paper is to propose a fractional-order causal approximation model of RILD that leads to a novel theory to unify causal RILD models developed by researchers independent of each other.

The finding that the energy losses of many solid materials per strain cycle are proportional to the square of strain amplitude and independent of the strain rate over a considerable frequency range leads to the introduction of the concept of RILD. It is also referred to as structural damping, linear hysteretic damping, or ideal hysteretic damping [3,4,5,6].

Crandall [6] examined the impulse response of a structure incorporated with RILD, and elucidated that RILD is non-causal. Owing to its non-causality, it is impossible to achieve its exact realization by using physical devices, which hinders its practical applications to exploit its benefit in low-frequency structures.

Researchers developed approximation methods of RILD to overcome the non-causality issue. The first successful causal model that exhibits approximated rate-independent dissipation behavior was proposed by Biot [7]. Caughey [8] pointed out that Biot model could be constructed by arranging an infinite number of Maxwell elements in parallel, which was thought to be a special case of Maxwell-Wiechert model[9]. Makris[10] proposed a causal linear hysteretic model which yielded exact rate-independent dissipation behavior and showed that it approached to Biot model as the excitation frequency became high.

More recently, Muscolino *et al.*[11] used the Laguerre polynomial approximation method to the prediction of the dynamic response of different RILD models under deterministic and random excitations. Spanos and Tsavachidis[12] introduced time-domain methods to minimize the computational costs in the dynamic analyses of structures incorporated with Biot model. Muravskii[13,14] studied several nonlinear hysteretic models leading to rate-independent damping and then constructed a causal linear model which exhibited nearly rate-independent dynamic stiffness by considering the structural system as a whole. Nakamura[15] proposed a causal model having a nearly constant loss modulus over piecewise frequency ranges. Genta and Amanti[16] proposed a tuned Maxwell-Wiechert (TMW) model that could mimic the loss modulus of RILD over a frequency range of interest, although limited number of Maxwell elements were used. For nonlinear dynamic analyses of rate-independently damped systems, Huang *et al.*[17] presented a causal model to mimic RILD, which reduced to a TMW model in a linear case.

Keivan *et al.*[18,19] proposed semi-active control methods to mimic the behavior of RILD by using a first-order causal digital filter, which was further passively realized by using a mechanical system consisting of a negative stiffness element coupled in parallel with a Maxwell element[2]. In the present study, to improve the approximation of the dissipation behavior of RILD, a novel model is proposed by generalizing the first-order causal filter into a fractional-order one, and several methods are suggested to physically realize the proposed model.

Although some attempts have already been made to mimic RILD by virtue of fractional-order models[20,21], to the best knowledge of the authors, there are no discussions on the relationships between a fractional-order model and existing causal ones for RILD. The novelty of this study lies in the insightfull finding of the relationships between the proposed model and existing causal models that lead to a novel theory to unifying causal RILD models.

The remainder of this paper is organized as follows. In Section 2, a review on well-known causal RILD approximation models are given. The frequency- and time-domain representations of the proposed model are given in Section 3 followed by the discussions on the relations between the proposed model with well-known causal RILD models in Section 4. Then, in Section 6, a time-domain method is developed for the dynamic analysis of structure systems incorporated with the proposed model, and several numerical examples (both linear and nonlinear types) are used to verify the effectiveness of the developed method. Finally, some conclusions are presented.

2 | MATHEMATICAL MODELS FOR RILD

This section presents mathematical models of non-causal and causal RILD, followed by the derivations of their dynamic stiffnesses, damping functions, damping kernel functions, and resistive force functions.

2.1 | A complex-stiffness model to represent ideal RILD

Consider a complex stiffness consisting of a linear main spring and a RILD element coupled in parallel as shown in Fig. 1. Its transfer function from deformation to the resistive force, also referred to as the dynamic stiffness is

$$\mathscr{H}_{\mathrm{I}}(i\omega) = \frac{F(i\omega)}{X(i\omega)} = k_0\left[1 + \eta \mathcal{Z}_{\mathrm{I}}(i\omega)\right] \tag{1}$$

where k_0 and η denote spring stiffness and loss factor, respectively. $\mathcal{Z}_{\mathrm{I}}(i\omega)$ denotes normalized dynamic stiffness of a RILD element, also known as a damping function. It can be expressed as follows,

$$\mathcal{Z}_{\mathrm{I}}(i\omega) = i\,\mathrm{sgn}(\omega) \tag{2}$$

where $i = \sqrt{-1}$ and $\mathrm{sgn}(\cdot)$ denotes the imaginary unit and the signum function, respectively. Applying an inverse Fourier transform to Eq.(2) gives[22]

$$z_{\mathrm{I}}(t) = \mathscr{F}^{-1}[\mathcal{Z}_{\mathrm{I}}(i\omega)] = -\frac{1}{\pi t} \tag{3}$$

where $\mathscr{F}^{-1}(\cdot)$ denotes the inverse Fourier transform. The above equation implies that this model is non-causal because it yields non-zero response force prior to the application of an impulse deformation, *i.e.*, $z_{\mathrm{I}}(t < 0) \neq 0$[23].

A damping kernel function can be obtained from an inverse Fourier transform of the impedance function. Because the impedance function is a transfer function from velocity to damping force, it is $\mathcal{Z}_{\mathrm{I}}(i\omega)/i\omega$. Thus, the damping kernel function of

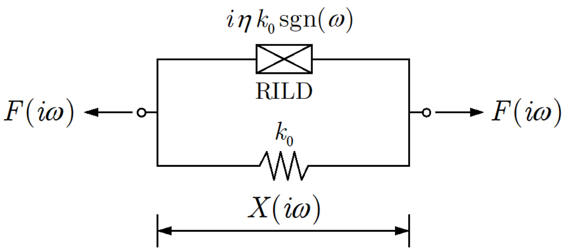

FIGURE 1 A complex-stiffness model

this model is derived as follows,

$$q_{\mathrm{I}}(t) = \mathscr{F}^{-1}\left[\frac{\mathcal{Z}_{\mathrm{I}}(i\omega)}{i\omega}\right] = -\frac{1}{\pi}\ln|t| \tag{4}$$

It is worth noting that the following relationship holds:

$$\frac{d}{dt}q_{\mathrm{I}}(t) = z_{\mathrm{I}}(t) \tag{5}$$

The resistive force generated by this non-causal model from a deformation $x(t)$ can be expressed as follows,

$$f_{\mathrm{I}}(t) = k_0 x(t) * \left[\delta(t) + \eta\, z_{\mathrm{I}}(t)\right] = k_0\left[x(t) + \eta\, \hat{x}(t)\right] \tag{6}$$

where the asterisk $*$ indicates the convolution integral. $\delta(t)$ denotes the Dirac's delta function, which is defined as an inverse Fourier transform of unity. The hat $'\hat{}\,'$ indicates the Hilbert transform, which can be expressed as follows[23,24],

$$\hat{x}(t) = -\frac{1}{\pi}\int_{-\infty}^{\infty}\frac{x(\tau)}{t-\tau}d\tau \tag{7}$$

This again shows that this model is non-causal because its resistive force depends on not only the past input deformations, but also those in the future.

The difficulty in conducting numerical analysis on a nonlinear system incorporated with a non-causal model demands the development of causal models.

2.2 | Biot model

Biot[7] proposed the first causal model yielding approximated rate-independent dissipation behavior. Caughey[8] pointed out that Biot model was physically represented by using an infinite number of Maxwell elements coupled in parallel. Such a representation is thought to be a special case of a Maxwell-Wiechert model shown in Fig. 2 with the number of Maxwell elements tends to infinity. In Fig. 2, c_j and k_j denote the damping coefficient and stiffness of the j-th Maxwell element, respectively; v_j denotes the deformation of the j-th damping element.

For the Maxwell-Wiechert model shown in Fig. 2, the dynamic stiffness is written as follows,

$$\mathscr{H}(i\omega) = k_0 + \sum_{j=1}^{n} k_j \frac{i\omega}{i\omega + r_j} \tag{8}$$

where r_j denotes the ratio of the spring stiffness and damping coefficient of the j-th Maxwell element, *i.e.*, $r_j = k_j/c_j$, which is also known as relaxation frequency or the inverse of the relaxation time.

It can be shown that as $n \to \infty$, the Maxwell-Wiechert model reduces to Biot model. To this end, it is assumed that the incremental relaxation frequencies of neighboring Maxwell elements are uniformly distributed, *i.e.*, $\Delta r = r_{j+1} - r_j$ $(j = 1, 2, \ldots, n)$. Determine the stiffness of the j-th Maxwell element such that

$$k_j = k_1\frac{\Delta r}{r_j} \tag{9}$$

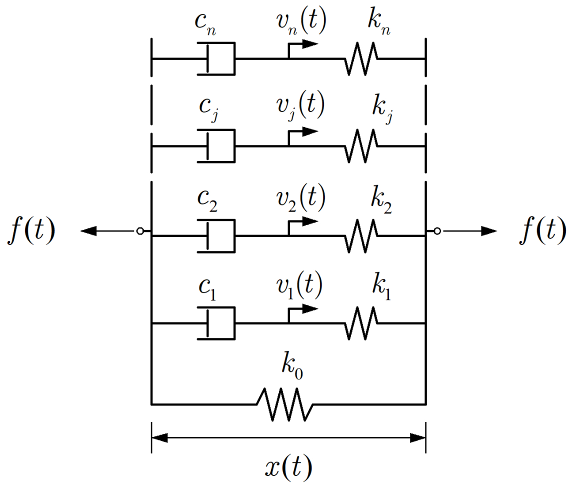

FIGURE 2 Maxwell-Wiechert model

where $k_1 = 2\eta k_0/\pi$. The dynamic stiffness of the designed Maxwell-Wiechert model can then be expressed as follows

$$\mathscr{H}(i\omega) = k_0 \left(1 + \frac{2\eta}{\pi} \sum_{j=1}^{n} \frac{i\omega}{i\omega + r_j} \frac{\Delta r}{r_j} \right) \tag{10}$$

Provided that $r_1 = \varepsilon$ and $\Delta r = r_a/\sqrt{n}$, where r_a is an arbitrary positive parameter having a dimension of circular frequency. As $n \to \infty$, one has $r_n = \varepsilon + (n-1)\Delta r \to \infty$ and $\Delta r = dr$, and then the above equation can be expressed as follows,

$$\mathscr{H}(i\omega) = k_0 \left(1 + \frac{2\eta}{\pi} \int_{\varepsilon}^{\infty} \frac{i\omega}{i\omega + r} \frac{dr}{r} \right) \tag{11}$$

Performing the integration in Eq.(11) in terms of its real and imaginary parts, respectively, gives the dynamic stiffness of Biot model as follows,

$$\mathscr{H}_{\mathrm{B}}(i\omega) = k_0 \left\{ 1 + \frac{2\eta}{\pi} \left[\ln \sqrt{1 + \left(\frac{\omega}{\varepsilon}\right)^2} + i \arctan\left(\frac{\omega}{\varepsilon}\right) \right] \right\} \tag{12}$$

where $\arctan(\cdot)$ denotes the inverse tangent function. By introducing the principal branch of the complex logarithm function $\ln(1 + i\omega/\varepsilon)$, one can rewrite Eq.(12) in a more compact form

$$\mathscr{H}_{\mathrm{B}}(i\omega) = k_0 \left[1 + \frac{2\eta}{\pi} \ln\left(1 + \frac{i\omega}{\varepsilon}\right) \right] \tag{13}$$

Corresponding to Eq.(1), the dynamic stiffness of Biot model can be reformulated as follows,

$$\mathscr{H}_{\mathrm{B}}(i\omega) = k_0 \left[1 + \eta \mathcal{Z}_{\mathrm{B}}(i\omega) \right] \tag{14}$$

where the damping function of Biot model can be respectively obtained from Eqs.(11)-(13) as follows,

$$\begin{aligned} \mathcal{Z}_{\mathrm{B}}(i\omega) &= \frac{2}{\pi} \int_{\varepsilon}^{\infty} \frac{i\omega}{i\omega + r} \frac{dr}{r} \\ &= \frac{2}{\pi} \left[\ln \sqrt{1 + \left(\frac{\omega}{\varepsilon}\right)^2} + i \arctan\left(\frac{\omega}{\varepsilon}\right) \right] \\ &= \frac{2}{\pi} \ln\left(1 + \frac{i\omega}{\varepsilon}\right) \end{aligned} \tag{15}$$

From the first equality in Eqs.(15), one can readily obtain the damping kernel function of Biot model as follows,

$$q_{\mathrm{B}}(t) = \mathscr{F}^{-1}\left[\frac{\mathcal{Z}_{\mathrm{B}}(\omega)}{i\omega} \right] = -\frac{2}{\pi} \mathrm{Ei}(-\varepsilon t) u(t) \tag{16}$$

where $u(t)$ denotes Heaviside's unit step function (*i.e.*, $u(t) = 0$, if $t \leq 0$; otherwise, $u(t) = 1$); $\mathrm{Ei}(-\varepsilon t)$ denotes the exponential integral, which can be expressed as follows[25],

$$\mathrm{Ei}(-\varepsilon t) = \int_{\varepsilon}^{\infty} \frac{-1}{e^{rt}} \frac{dr}{r} = \ln|\varepsilon t| + \gamma_0 + \sum_{n=1}^{\infty} \frac{(-1)^n(\varepsilon t)^n}{n\, n!} \tag{17}$$

where $\gamma_0 \doteq 0.577$ is the Euler constant.

Thus, the resistive force generated by Biot model can then be obtained as follows,

$$f_{\mathrm{B}}(t) = k_0[x(t) + \eta\, \dot{x}(t) * q_{\mathrm{B}}(t)] \tag{18}$$

Substituting Eq.(16) into the above equation gives

$$f_{\mathrm{B}}(t) = k_0 \left\{ x(t) - \frac{2\eta}{\pi} \dot{x}(t) * [\mathrm{Ei}(-\varepsilon t)u(t)] \right\} \tag{19}$$

which coincides with the time-domain representation of Biot model given by Caughey[8].

2.3 | Makris model

An alternative explanation for the non-causality of the complex-stiffness model is that the real and imaginary parts of its dynamic stiffness fail to relate with each other by Hilbert transform. Such relations, referred to as Kramers-Kronig relation, are known as the sufficient and necessary condition for a strictly proper transfer function to ensure the causality in the strict sense[26].

By modifying the real part of Eq.(2) into the Hilbert transform of its imaginary part in order to satisfy causality requirement, Makris[10] constructed a causal model having a dynamic stiffness as follows,

$$\mathscr{H}_{\mathrm{M}}(i\omega) = k_0 \left[1 + \eta\, \mathcal{Z}_{\mathrm{M}}(i\omega)\right] \tag{20}$$

where the damping function of this model is given as follows,

$$\mathcal{Z}_{\mathrm{M}}(i\omega) = \frac{2}{\pi} \ln\left|\frac{\omega}{\varepsilon}\right| + i\ \mathrm{sgn}\left(\frac{\omega}{\varepsilon}\right) \tag{21}$$

Similar to the case of Biot model, by introducing the principal branch of the complex logarithm function $\ln(i\omega/\varepsilon)$, the above equation can be expressed in more compact form as follows,

$$\mathcal{Z}_{\mathrm{M}}(i\omega) = \frac{2}{\pi} \ln\left(\frac{i\omega}{\varepsilon}\right) \tag{22}$$

It may be noticed that the last term in Eq.(15) approaches to Eq.(22) when $\omega \gg \varepsilon$, which means that Makris and Biot models behave similarly in high-frequency regions. In aother word, Biot model can be used as an approximation of Makris model[10] in a high frequency region. Applying an inverse Fourier transform to Eq.(21) in the sense of generalized function[27] gives

$$z_{\mathrm{M}}(t) = \mathscr{F}^{-1}\left[\mathcal{Z}_{\mathrm{M}}(i\omega)\right] = -\frac{2u(t)}{\pi t} \tag{23}$$

The damping kernel function of this model is[10],

$$q_{\mathrm{M}}(t) = \mathscr{F}^{-1}\left[\frac{\mathcal{Z}_{\mathrm{M}}(i\omega)}{i\omega}\right] = -\frac{2}{\pi}\left(\ln|\varepsilon t| + \gamma_0\right) u(t) \tag{24}$$

It is worth noting that Eq.(16) reduces to the above equation as εt tends to zero (so that the last term in Eq.(17) vanishes). The resistive force provided by Makris model from a deformation $x(t)$ can be obtained as follows,

$$f_{\mathrm{M}}(t) = k_0 \left[x(t) + \eta\, \dot{x}(t) * q_{\mathrm{M}}(t)\right] \tag{25}$$

Substituting Eq.(24) into the above equation gives

$$f_{\mathrm{M}}(t) = k_0 \left\{ \left(1 - \frac{2\eta}{\pi}\gamma_0\right) x(t) - \frac{2\eta}{\pi} \dot{x}(t) * [\ln|\varepsilon t| u(t)] \right\} \tag{26}$$

which includes a negative constant term in the displacement-dependent part. This suggests that a negative stiffness element can be used in the physical approximation of RILD[28,29].

2.4 | Tuned Maxwell-Wiechert model

For numerical implementation, a Prony series with a finite number of exponential relaxation functions was used by Makris and Zhang[30] to approximate the behavior of Biot model. Such a series is also known as the relaxation modulus or damping kernel function of a Maxwell-Wiechert model, as shown in Fig. 2. Furthermore, a Prony series was used by Spanos and Tsavachidis[12] to develop a recursive procedure for dynamic analysis of structural systems incorporated with Biot model. Genta and Amati[16] proposed the concept of tuned Maxwell-Wiechert (TMW) model so that its loss moduli can fit those of the non-causal RILD over a frequency range of interest. Similar concept was later used by Reggio *et al.*[31] for system identification applications and used by Huang *et al.*[17] in nonlinear analysis of rate-independently damped structures.

The dynamic stiffness of a TMW model is given as follows,

$$\mathscr{H}_{\mathrm{T}}(i\omega) = k_0 \left[1 + \eta \mathcal{Z}_{\mathrm{T}}(i\omega)\right] \tag{27}$$

where the damping function is given as follows,

$$\mathcal{Z}_{\mathrm{T}}(i\omega) = \sum_{j=1}^{n} \phi_j \frac{i\omega}{i\omega + r_j} \tag{28}$$

where ϕ_j is an adjusting parameter with respect to a discrete frequency point $\omega = r_j$, or physically represents the normalized stiffness of the j-th Maxwell element with a relaxation frequency of r_j. The damping kernel function of this model is written as follows,

$$q_{\mathrm{T}}(t) = \mathscr{F}^{-1}\left[\frac{\mathcal{Z}_{\mathrm{T}}(i\omega)}{i\omega}\right] = \sum_{j=1}^{n} \phi_j e^{-r_j t} u(t) \tag{29}$$

With sufficient terms, Eq.(29) can be used to approximate any physical relaxation process. With a target function, a regression analysis can be conducted to determine the parameters ϕ_j and r_j $(j = 1, 2, \dots, n)$, and both frequency- and time-domain methods[32] are available for this purpose.

With Eq.(29), the resistive force generated by a TMW model can be expressed as follows,

$$f_{\mathrm{T}}(t) = k_0 \left[x(t) + \eta \dot{x}(t) * \sum_{j=1}^{n} \phi_j e^{-r_j t} u(t)\right] \tag{30}$$

The above model is thought to be suitable for numerical implementation, because some available commercial softwares provide entrances for the parameters ϕ_j and r_j $(j = 1, 2, \dots, n)$.

3 | THE PROPOSED MODEL FOR RILD

3.1 | A fractional-order causal model

An alternative way that is recently developed to approximate ideal RILD (Eq. 2) is to use the first-order all-pass filter[18] defined as follows

$$\mathcal{Z}_1(i\omega) = \frac{i\omega - \varepsilon}{i\omega + \varepsilon} \tag{31}$$

which produces unity amplitude all over the frequency and an equal phase lead of $\pi/2$ rad at $\omega = \varepsilon$ same as ideal RILD. However, the above filter suffers strong rate-dependency in loss modulus, which may compromise its capability to simulate the energy dissipation behavior of RILD over a broad frequency range.

Here, the first-order causal filter is generalized and extended to a fractional-order filter defined in the following form

$$\mathcal{Z}_\alpha(i\omega) = \beta_\alpha \frac{(i\omega)^\alpha - \varepsilon^\alpha}{(i\omega)^\alpha + \varepsilon^\alpha} \tag{32}$$

where the real-valued parameter α is defined within the range $[0, 1]$. The power of a complex value $(i\omega)^\alpha$ is defined over the principal branch as follows,

$$(i\omega)^\alpha = |\omega|^\alpha \exp[i\ \alpha\ \mathrm{sgn}(\omega)\ \pi/2] \tag{33}$$

and β_α is a real-valued adjusting coefficient. For example, letting the amplitude of the filter be adjusted to unity (*i.e.* the same as ideal RILD defined in Eq.(2)) at $\omega = \varepsilon$ gives

$$\beta_\alpha = \cot\left(\frac{\alpha\pi}{4}\right) \tag{34}$$

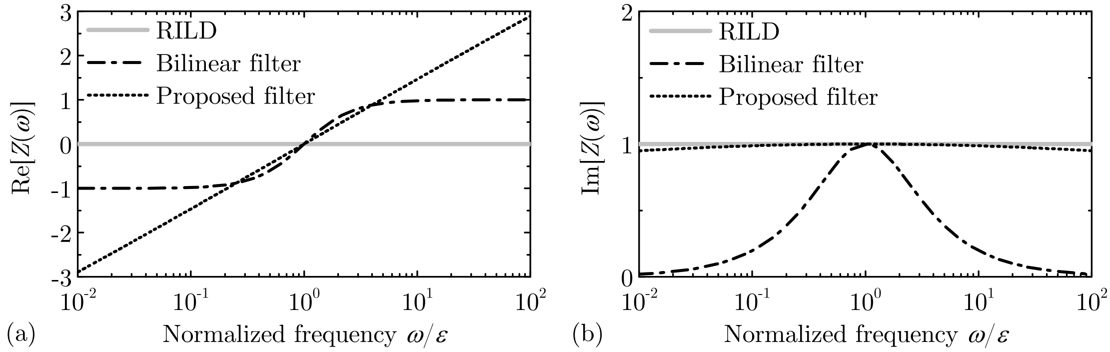

FIGURE 3 Comparison between the damping functions of different elements: (a) real and (b) imaginary parts.

where $\cot(\cdot)$ indicates the cotangent function. A novel factional-order filter is then proposed as follows,

$$\mathcal{Z}_\alpha(i\omega) = \cot\left(\frac{\alpha\pi}{4}\right)\frac{(i\omega)^\alpha - \varepsilon^\alpha}{(i\omega)^\alpha + \varepsilon^\alpha} \tag{35}$$

which reduces to Eq.(31) as α tends to unity.

Compared with the first-order causal filter, the proposed filter can provide a less rate-dependent loss modulus over a considerable frequency range. For example, Fig. 3 compares the real and imaginary parts of the proposed filter (*e.g.*, $\alpha = 0.1$), the first-order causal filter, and ideal RILD. It is shown that the proposed filter (*e.g.*, $\alpha = 0.1$) provides an improved approximation of RILD in terms of loss modulus, while yielding similar storage moduli to those of a first-order causal filter over a frequency range near $\omega = \varepsilon$.

Corresponding to the complex-stiffness model given in Eq.(1), the proposed model for RILD is constructed with a dynamic stiffness as follows,

$$\mathscr{H}_\alpha(i\omega) = k_0[1 + \eta\, \mathcal{Z}_\alpha(i\omega)] \tag{36}$$

From the equation above, we can understand that the fractional-order filter $\mathcal{Z}_\alpha(i\omega)$ (Eq.(35)) is a damping function.

3.2 | Causality of the proposed model

Here, the causality of the proposed model is first investigated. To this end, letting $0 < \alpha < 1$, the damping function of the proposed model is reformulated as follows,

$$\mathcal{Z}_\alpha(i\omega) = \beta_\alpha\,[2i\omega\mathscr{G}(i\omega) - 1] \tag{37}$$

where an auxiliary function $\mathscr{G}(i\omega) = (i\omega)^{\alpha-1}/[(i\omega)^\alpha + \varepsilon^\alpha]$ is introduced. The damping kernel function of the proposed model can be obtained from an inverse Fourier transform of the impedance function as follows,

$$q_\alpha(t) = \mathscr{F}^{-1}\left[\frac{\mathcal{Z}_\alpha(i\omega)}{i\omega}\right] = \beta_\alpha\,[2g(t) - u(t)] \tag{38}$$

where $g(t)$ denotes an inverse Fourier transform of $\mathscr{G}(i\omega)$, *i.e.*

$$g(t) = \mathscr{F}^{-1}[\mathscr{G}(i\omega)] = \frac{1}{2\pi}\int_{-\infty}^{\infty}\frac{(i\omega)^{\alpha-1}}{(i\omega)^\alpha + \varepsilon^\alpha}e^{i\omega t}d\omega \tag{39}$$

Note that, for $0 < \alpha < 1$, the denominator of the integrand of the above equation

$$(i\omega)^\alpha + \varepsilon^\alpha = |\omega|^\alpha\left[\cos(\alpha\pi/2) + i\,\mathrm{sgn}(\omega)\sin(\alpha\pi/2)\right] + \varepsilon^\alpha$$

has positive real and imaginary parts, *i.e.*, $(i\omega)^\alpha + \varepsilon^\alpha \neq 0$ for any ω when $0 < \alpha < 1$. Therefore, the integrand $\mathscr{G}(i\omega)$ has no pole, and thus the residual terms vanish when the Cauchy integration theorem is applied to evaluate the integral in Eq.(39).

In the case of $t < 0$, one can readily verify $g(t < 0)$ vanishes by virtue of the Jordan's lemma[33], and thus one has $q_\alpha(t < 0) \equiv 0$. This means that the proposed model is causal, and can be realized by using physical systems.

3.3 | Time-domain representation

Next, for $t > 0$, the time-domain representation of the proposed model is derived as follows. Letting $s = i\omega$, one can reformulate Eq.(39) as follows,

$$g(t) = \frac{1}{2\pi i}\int_{-i\infty}^{i\infty} \frac{s^{\alpha-1}}{s^\alpha + \varepsilon^\alpha} e^{st} ds = \mathscr{L}^{-1}\left[\frac{s^{\alpha-1}}{s^\alpha + \varepsilon^\alpha}\right] \tag{40}$$

where $\mathscr{L}^{-1}(\cdot)$ indicates the inverse Laplace transform. It is well established that[34]

$$\frac{s^{\alpha-1}}{s^\alpha + 1} = \mathscr{L}\left[E_\alpha(-t^\alpha)\right] \tag{41}$$

where $E_\alpha(-t^\alpha)$ denotes the Mittag-Leffler relaxation function, which can be defined as follows,

$$E_\alpha(-t^\alpha) = \sum_{n=0}^{\infty} \frac{(-1)^n t^{\alpha n}}{\Gamma(\alpha n + 1)} \tag{42}$$

where $\Gamma(\cdot)$ denotes the Euler's Gamma function. Recall that $g(t < 0) \equiv 0$, from Eqs.(40) and (41), one can readily obtain

$$g(t) = E_\alpha(-\varepsilon^\alpha t^\alpha)u(t) \tag{43}$$

Substituting Eq.(43) into Eq.(38) gives the damping kernel function of the proposed model as follows,

$$q_\alpha(t) = \beta_\alpha u(t)\left[2E_\alpha(-\varepsilon^\alpha t^\alpha) - 1\right] \tag{44}$$

Then, the resistive force $f_\alpha(t)$ generated by the proposed model is obtained as follows,

$$f_\alpha(t) = k_0\left[x(t) + \eta\, \dot{x}(t) * q_\alpha(t)\right] \tag{45}$$

Substituting Eq.(44) into the above equation gives

$$f_\alpha(t) = k_0\left\{(1-\eta\beta_\alpha)x(t) + 2\eta\beta_\alpha \dot{x}(t) * \left[E_\alpha(-\varepsilon^\alpha t^\alpha)u(t)\right]\right\} \tag{46}$$

With $\alpha = 1$, one has $E_\alpha(-\varepsilon^\alpha t^\alpha) = e^{-\varepsilon t}$ and $\beta_\alpha = 1$, and thus it follows that

$$f_\alpha(t) = k_0\left\{(1-\eta)x(t) + 2\eta\dot{x}(t) * \left[e^{-\varepsilon t}u(t)\right]\right\} \tag{47}$$

which represents the resistive force generated by Keivan model[18]. It is worth noting that the negative constant term $-\eta$ in the displacement dependent part correspond to a negative stiffness element used in the physical realization of RILD discussed by Luo *et al.*[2].

4 | A UNIFYING FRAMEWORK OF RILD

For comparison, Table 1 summarizes the damping functions and kernel functions of different models for RILD introduced above. The relationships between the proposed and those existing causal models listed in Table 1 are discussed in the following.

4.1 | Relaionship with Makris model

Here, it is proved that the proposed model can include Makris model as a special case of $\alpha = 0$. Letting $\lambda = \omega/\varepsilon$, one can reformulate Eq.(35) as follows,

$$\mathcal{Z}_\alpha(i\lambda) = \frac{\cos(\alpha\pi/4)\{(i\lambda)^\alpha - 1\}}{\sin(\alpha\pi/4)\{(i\lambda)^\alpha + 1\}} \tag{48}$$

Because both the denominator and numerator of the above equation approach to 0 as α approaches to 0, the l'Hôpital's rule is applied to obtain the limit

$$\lim_{\alpha\to 0} \mathcal{Z}_\alpha(i\lambda) = \lim_{\alpha\to 0} \frac{-(\pi/4)\sin(\alpha\pi/4)\{(i\lambda)^\alpha - 1\} + \cos(\alpha\pi/4)\{\ln(i\lambda)\cdot(i\lambda)^\alpha\}}{(\pi/4)\cos(\alpha\pi/4)\{(i\lambda)^\alpha + 1\} + \sin(\alpha\pi/4)\{\ln(i\lambda)\cdot(i\lambda)^\alpha\}} = \frac{2}{\pi}\ln(i\lambda) \tag{49}$$

Recall that $\lambda = \omega/\varepsilon$, one can reformulate the above equation as follows,

$$\lim_{\alpha\to 0} \mathcal{Z}_\alpha(i\omega) = \frac{2}{\pi}\ln\left(\frac{i\omega}{\varepsilon}\right) = \frac{2}{\pi}\ln\left|\frac{\omega}{\varepsilon}\right| + i\,\mathrm{sgn}\left(\frac{\omega}{\varepsilon}\right) \tag{50}$$

TABLE 1 Comparison of different RILD elements

Model	Damping function $\mathcal{Z}(i\omega)$	Damping kernel function $q(t)$	Causality
RILD	$i\ \mathrm{sgn}(\omega)$	$-\frac{1}{\pi}\ln\lvert t\rvert$	Non-Causal
Biot	$\frac{2}{\pi}\ln\left(1+i\frac{\omega}{\varepsilon}\right)$	$-\frac{2u(t)}{\pi}\mathrm{Ei}(-\varepsilon t)$	Causal
Makris	$\frac{2}{\pi}\ln\left(\frac{i\omega}{\varepsilon}\right)$	$-\frac{2u(t)}{\pi}\left(\ln\lvert\varepsilon t\rvert+\gamma_0\right)$	Causal
TMW	$\sum_{j=1}^{n}\phi_j\frac{i\omega}{i\omega+r_j}$	$\sum_{j=1}^{n}u(t)\phi_j e^{-r_j t}$	Causal
Keivan	$\frac{i\omega-\varepsilon}{i\omega+\varepsilon}$	$u(t)\left[2e^{-\varepsilon t}-1\right]$	Causal
Proposed	$\beta_\alpha\frac{(i\omega)^\alpha-\varepsilon^\alpha}{(i\omega)^\alpha+\varepsilon^\alpha}$	$\beta_\alpha u(t)\left[2E_\alpha(-\varepsilon^\alpha t^\alpha)-1\right]$	Causal

which coincides with the damping function of Makris model, as defined in Eqs.(21) and (22).

The coincidence between the damping function of the two models in the frequency domain also suggests that the damping kernel function of the proposed model in the case of $\alpha = 0$ can be expressed as Eq.(24). Furthermore, because the dynamic stiffness and damping kernel function of the proposed model vary continuously with the value of α, it can also be predicted that the proposed model with a small order of α (*e.g.*, $\alpha = 0.1$) can provide a good approximation of Makris model, at least over a frequency range of interest.

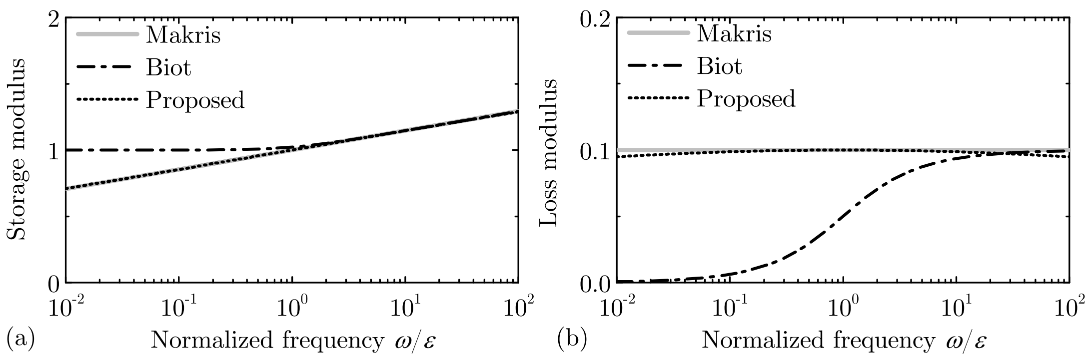

FIGURE 4 Comparison between the normalized dynamic stiffnesses of different models for RILD ($\eta = 0.1$)

For example, letting $\eta = 0.1$, Fig. 4 compares the normalized dynamic stiffness of the proposed model (*e.g.*, $\alpha = 0.1$) with those of the Makris and Biot models. It is shown in Fig. 4 that the differences between the dynamic stiffness of the proposed model with $\alpha = 0.1$ and that of Makris model are negligible over a considerable frequency range. This means that the proposed model with a small order of α can be used to approximate Makris model without significant loss of accuracy. It should be mentioned that in some cases, such an approximation seems to be necessary and useful, as to be further discussed in Section 5.

4.2 | Relationship with Biot model

Here, it is first shown that the proposed model is equivalent to a first-order approximation of Biot model in terms of dynamic stiffness as the order α tends to unity (*i.e.*, Keivan model). To this end, one can rewrite Eq.(15) as follows,

$$\mathcal{Z}_{\mathrm{B}}(i\omega) = \frac{2}{\pi}\left[\ln 2 - \ln\left(1 - \frac{i\omega - \varepsilon}{i\omega + \varepsilon}\right)\right] \tag{51}$$

By using the Mercator series to expand the frequency-dependent term (the second ln( ) term) in the above equation, one can obtain

$$\mathcal{Z}_{\mathrm{B}}(i\omega) = \frac{2}{\pi}\left[\ln 2 + \sum_{n=1}^{\infty}\frac{1}{n}\left(\frac{i\omega - \varepsilon}{i\omega + \varepsilon}\right)^{n}\right] \tag{52}$$

Then, substituting Eq.(52) into Eq.(14) gives an alternative expression for the dynamic stiffness of Biot model as follows,

$$\mathscr{H}_{\mathrm{B}}(i\omega) = k_0\left[1 + \frac{2\eta}{\pi}\ln 2 + \frac{2\eta}{\pi}\sum_{n=1}^{\infty}\frac{1}{n}\left(\frac{i\omega - \varepsilon}{i\omega + \varepsilon}\right)^{n}\right] \tag{53}$$

Letting $\bar{k}_0 = k_0[1 + (2\eta\ln 2)/\pi]$ and $\bar{\eta} = 2\eta/(\pi + 2\eta\ln 2)$, one can rewrite Eq.(53) as follows,

$$\mathscr{H}_{\mathrm{B}}(i\omega) = \mathscr{H}_{\mathrm{B}}^{(N)}(i\omega) + \bar{\eta}\,\bar{k}_0\sum_{n=N+1}^{\infty}\frac{1}{n}\left(\frac{i\omega - \varepsilon}{i\omega + \varepsilon}\right)^{n} \tag{54}$$

where $\mathscr{H}_{\mathrm{B}}^{(N)}(i\omega)$ denotes the Nth-order truncated approximation of $\mathscr{H}_{\mathrm{B}}(i\omega)$, and can be expressed as follows,

$$\mathscr{H}_{\mathrm{B}}^{(N)}(i\omega) = \bar{k}_0\left[1 + \bar{\eta}\sum_{n=1}^{N}\frac{1}{n}\left(\frac{i\omega - \varepsilon}{i\omega + \varepsilon}\right)^{n}\right] \tag{55}$$

Letting $N = 1$, one has

$$\mathscr{H}_{\mathrm{B}}^{(1)}(i\omega) = \bar{k}_0\left(1 + \bar{\eta}\,\frac{i\omega - \varepsilon}{i\omega + \varepsilon}\right) \tag{56}$$

which has the same form as the dynamic stiffness of the proposed model expressed in Eq.(36) with $\alpha = 1$ (*i.e.*, Keivan model). This means that Keivan model is actually equivalent to a first-order approximation of Biot model.

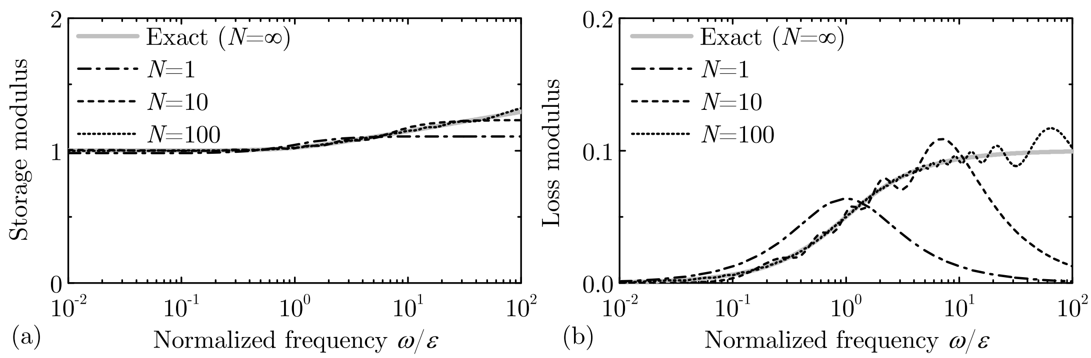

FIGURE 5 Approximation of the dynamic stiffness of Biot model by using Mercator series ($\eta = 0.1$)

To further investigate the effect of N on the accuracy to approximate the dynamic stiffness of Biot model, for example, letting $\eta = 0.1$, Fig. 5 compares the Nth-order truncated approximation of normalized dynamic stiffness of Biot model with $N = 1, 10, 100$, and ∞, respectively. It is shown in Fig. 5 that a first-order approximation exhibits similar characteristics of the dynamic stiffness of Biot model in low frequency region; in order to capture the high-frequency characteristics of Biot model, a much higher-order approximation is required. Alternatively, the proposed model with a small order α (*e.g.*, $\alpha = 0.1$) can be used, at the expense of distorted low-frequency characteristics.

As mentioned in Section 2, the dynamic stiffness of Biot model approaches to that of Makris model when $\omega \gg \varepsilon$. Thus, from the revealed relation between the proposed and Makris models, the proposed model with a small order α (*e.g.*, $\alpha = 0.1$) can also be used to approximate the high-frequency characteristics of Biot model. As shown in Fig. 4, the proposed model behaves similarly as Biot model in high frequency region.

4.3 | Equivalence to a modified TMW model

Here, it is shown that the proposed model is equivalent to a TMW model with its storage modulus modified by a rate-independent term. To this end, quantified comparisons between the TMW and proposed models are made, and the method suggested by Huang *et al.*[17] is used to design the order of TMW model, ϕ_j, with respect to a given set of r_j, $j = 1, 2, ..., n$, which are logarithmically spaced over a frequency range from 0.01ε to 100ε. Two different TMW models are designed with $n = 5$, and $n = 7$, respectively.

In order to approximate the non-causal model represented by Eq.(1) at a specified frequency $\omega = \varepsilon$, here, the dynamic stiffness of TMW model is modified as follows,

$$\mathscr{H}_{\mathrm{T}}'(i\omega) = k_0 \left[1 - \eta \mathcal{Z}_{\mathrm{Mod}}(\varepsilon) + \eta \mathcal{Z}_{\mathrm{T}}(i\omega)\right] \tag{57}$$

where $Z_{\mathrm{Mod}}(\varepsilon)$ is a rate-independent modification term, *i.e.*,

$$\mathcal{Z}_{\mathrm{Mod}}(\varepsilon) = \mathscr{R}\left[\mathcal{Z}_{\mathrm{T}}(i\varepsilon)\right] = \sum_{j=1}^{n} \frac{\phi_j \varepsilon^2}{\varepsilon^2 + r_j^2} \tag{58}$$

It should be mentioned that a modification by adding a rate-independent term to the storage modulus does not affect the causality of the original model (*e.g.*, see reference[15]). It can be physically interpreted as connecting the TMW model in parallel with a linear negative stiffness element whose absolute stiffness is $\eta k_0 Z_{\mathrm{Mod}}(\varepsilon)$, as done by the authors[2].

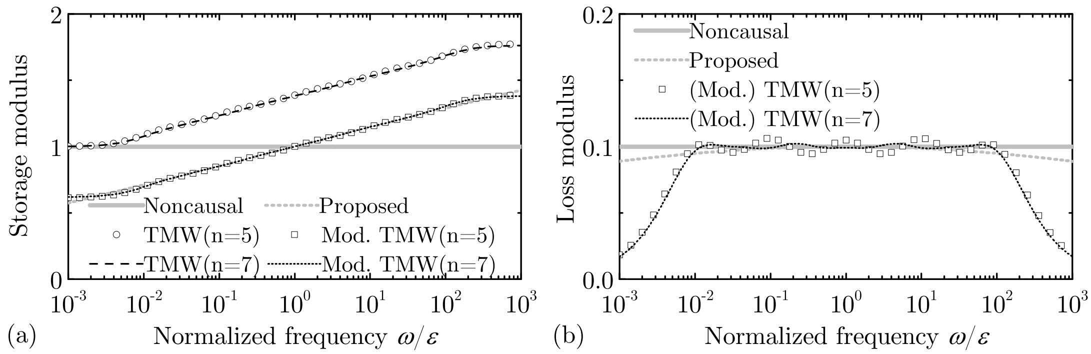

FIGURE 6 Comparison between the TMW and proposed models ($\eta = 0.1$)

Alternatively, one can also reformulate Eq.(57) as follows,

$$\mathscr{H}_{\mathrm{T}}'(i\omega) = k_0' \left[1 + \eta' \mathcal{Z}_{\mathrm{T}}(i\omega)\right] \tag{59}$$

where $k_0' = k_0 \left[1 - \eta Z_{\mathrm{Mod}}(\varepsilon)\right]$ and $\eta' = \eta / \left[1 - \eta Z_{\mathrm{Mod}}(\varepsilon)\right]$. The above equation has the same form as the dynamic stiffness of TMW model expressed in Eq.(27). This suggests that the modified model can be equivalently realized by designing a TMW model with k_0' and η' instead of k_0 and η, respectively. In other word, one can equivalently realize the modified model without supplementing a physical negative stiffness element.

To further illustrate the relationship between the TMW and proposed models, for example, letting $\eta = 0.1$, Fig. 6 depicts the normalized dynamic stiffnesses of TMW models, as well as those of the non-causal model and proposed model (*e.g.*, $\alpha = 0.1$) for comparison. It is shown that the accuracy of TMW model for approximating the loss modulus of non-causal model is improved as the number n increases. Moreover, modifying the storage modulus of TMW model to fit the non-causal model at $\omega = \varepsilon$ leads to a good fit to the proposed model over the frequency range of interest.

The modified TMW model can be equivalently represented by the proposed model to mimic the behavior of the non-causal RILD. This may be preferable in some applications because much reduced empirical parameters are used for simulations in the proposed model. The proposed model requires only one additional parameter α, whereas seven adjusting parameters ϕ_j

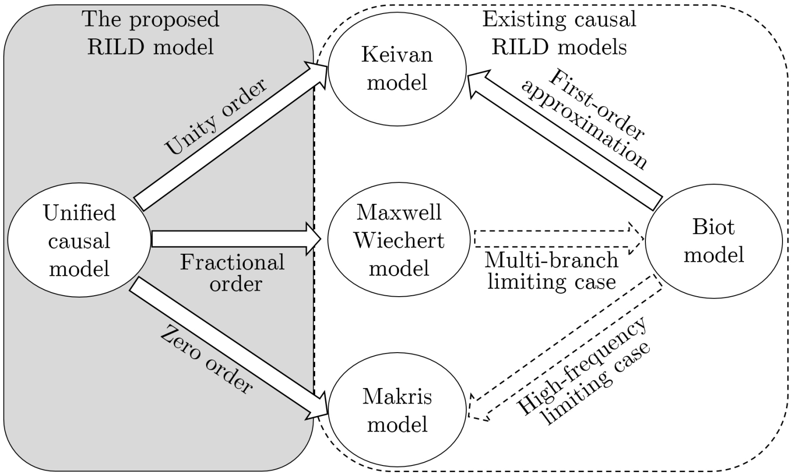

FIGURE 7 A new framework of causal models for RILD

($j = 1, 2, ..., 7$) are used for the (modified) TMW model so that it was equivalent to the proposed model in this example. This implies the advantage of the fractional-order operator over integer-order operators used in a constitutive law[35,36].

Each Maxwell element can be realized by connecting a viscous damper in series with a spring and then connected with each other in parallel to construct a TMW model. In this regard, the modified TMW model is considered as a viable option to physically realize the proposed model. Further discussions on the physical realization of the proposed model are given in Section 5.

In summary, the relationships between different causal models for RILD are shown in Fig. 7. It has been proved that the proposed model can include both Keivan and Makris models as its special cases with $\alpha = 1$ and $\alpha = 0$, respectively. From the comparison in Fig. 6, it is suggested that the proposed model with a fractional order (*e.g.*, $\alpha = 0.1$) is equivalent to a modified Maxwell Wiechert model, which is able to approximate Biot model for practical applications (*e.g.*, see references[12,30]). In this regard, the proposed model can be considered as a unifying causal model for RILD. Furthermore, in Subsection 4.2, Keivan model is shown to be equivalent to a first-order approximation of Biot model. These newly revealed relationships (indicated by solid arrows in Fig. 7), along with the established ones (indicated by dashed arrows in Fig. 7) between different models contribute to the development of a novel framework for causal models of RILD bringing insight to the nature of RILD .

5 | PHYSICAL REALIZATION OF RILD

Owing to its non-causality, RILD cannot be realized strictly by using real-life devices. However, it would be useful if we could physically realize approximated causal models that can exploit the benefit of RILD in practical applications. The authors have developed a mechanical system to physically realize the first-order causal filter by connecting a Maxwell element in parallel with a negative stiffness element[2]. This section discusses the further expansion of this method to examine the feasibility of the realization by using fractional-order model.

5.1 | A mechanical representation of the proposed model

Here, for physical realization of the proposed model, a mechanical representation is developed on the basis of our past study[2]. To this end, a conventional Maxwell element is generalized into a fractional-order one consisting of a linear spring arranged in series with a fractional-order damping element, as shown in Fig. 8, where k_α and k_N denote the stiffnesses of the fractional-order Maxwell and negative stiffness elements, respectively. $v(t)$ denotes the deformation of fractional-order damping element.

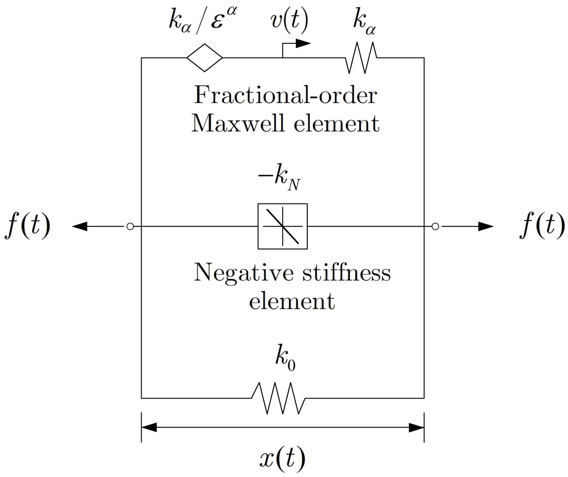

FIGURE 8 A mechanical representation of the proposed model

Here, it is to be shown that the dynamic stiffness of the mechanical representation in Fig. 8 is identical to that of the proposed model as shown in Eq. (57). The equilibrium equation of motion of the fractional-order Maxwell element can be expressed as follows,

$$k_\alpha\{x(t)-v(t)\} = \frac{k_\alpha}{\epsilon^\alpha} D^\alpha_{0+} v(t) \tag{60}$$

where $D^\alpha_{0+} v(t)$ denotes an α-order derivative of $v(t)$ with respect to t.

This reduces to

$$D^\alpha_{0+} v(t) + \varepsilon^\alpha v(t) = \varepsilon^\alpha x(t) \tag{61}$$

Here, the Riemann-Liouville's definition [37] of the fractional derivative is used and defined as follows,

$$D^\alpha_{0+} v(t) := \frac{1}{\Gamma(1-\alpha)} \frac{d}{dt} \int_0^t \frac{v(\tau)}{(t-\tau)^\alpha} d\tau \tag{62}$$

By using the property of fractional derivative [37], one has

$$\mathscr{F}[D^\alpha_{0+} v(t)] = (i\omega)^\alpha \mathscr{F}[v(t)] = (i\omega)^\alpha V(i\omega) \tag{63}$$

Thus, applying a Fourier transform to Eq.(61) gives

$$V(i\omega) = \frac{\varepsilon^\alpha}{(i\omega)^\alpha + \varepsilon^\alpha} X(i\omega) \tag{64}$$

The resistive force provided by the mechanical model in Fig. 8 can be written as follows,

$$f(t) = (k_0 - k_N)x(t) + k_\alpha[x(t) - v(t)] \tag{65}$$

Applying a Fourier transform to Eq.(65) gives

$$F(i\omega) = (k_0 - k_N)X(i\omega) + k_\alpha[X(i\omega) - V(i\omega)] \tag{66}$$

With $k_N = \eta\beta_\alpha k_0$ and $k_\alpha = 2\eta\beta_\alpha k_0$, substituting Eq.(64) into Eq.(66) gives its dynamic stiffness as follows,

$$\mathscr{H}(i\omega) = k_0 \left[1 + \eta\ \beta_\alpha \frac{(i\omega)^\alpha - \varepsilon^\alpha}{(i\omega)^\alpha + \varepsilon^\alpha}\right] \tag{67}$$

which coincides with the dynamic stiffness of the proposed model expressed in Eq.(36). This verifies that the proposed fractional-order filter can be represented by using a fractional-order Maxwell element in parallel with a negative stiffness element (hereafter referred to as fractional-Maxwell-negative-stiffness (FMNS) model).

5.2 | Feasibility of physical realizations

In terms of physical realization of the FMNS model, the negative stiffness element can be created by equivalently reducing the horizontal stiffness of the primary structure (or of isolators), or physically realized by using passive negative stiffness devices[38], as discussed in our past study[2]. With respect to the fractional-order Maxwell element, many engineering solid materials[35,36] and some damping devices[39,40] have been reported to be accurately simulated by using fractional-order damping elements. Therefore, it is straightforward to develop such real-life damping devices, which can physically realize the fractional-order element to be used in the FMNS model. In this regard, further challenges remain in developing real-life devices having desired damping characteristics.

Except for the above method, at present, two types of alternative methods are also thought to be promising in physical realization of the FMNS model: (i) to develop a passive system consisting of multiple existing damping devices, which is equivalent to the FMNS model (as discussed in Subsection 4.3. A modified TMW model is would be a viable option); or (ii) to employ semi-active devices[18], which can generate the desired damping force yielded by the FMNS model. An efficient time-domain calculation technique is required to ensure the real-time control based on FMNS model[41].

As the order α tends to unity, the fractional-order Maxwell element reduces to a conventional Maxwell element, and the FMNS model reduces to a Maxwell-negative-stiffness (MNS) model. The MNS model consisting of only one Maxwell element and one negative stiffness element, and thus is thought to be the simplest realizable case of the FMNS (or modified TMW) model. The application of MNS model used for seismic performance enhancement of base-isolated structures is discussed in our past study[2].

As the order α tends to zero, the fractional-order Maxwell element can be used to mechanically represent the damping (frequency-dependent) part of Makris model in the theoretical sense. However, an exact and physical realization of such an element is impossible in practical engineering applications because the required stiffnesses of negative stiffness element and Maxwell spring are infinite. Such elements having infinite stiffnesses can be even hard to be used in numerical simulation problems. Instead, the FMNS model with a small order α may be used for approximation, so that those parameters can be designed within a reasonable range. This suggests that the proposed model having an additional adjusting parameter α is a viable option for practical applications.

6 | CONCLUSIONS

Increasing damping in a structure is effective in reducing excessive displacements induced by low-frequency components of ground motion, which, however, might result in excessive damping force and floor response accelerations induced by high-frequency components. Using RILD is a promissing option to avoid compromized performance in reducing damping force and floor response accelerations when incorporating a high amount of damping because its damping force does not increase even if the excitation frequency increases. Indeed, RILD performs selective damping to effectively reduce displcement without increacing floor response accelerations when incorporated into a low-frequency structure.

In this study, a novel causal RILD model is proposed to exploit its benefit in low-frequency structures. The proposed model is obtained by modifying the order of Keivan model (first-order), into fractional-order. It is shown that the proposed model improves the approximation in energy dissipation behavior in a considerably wide frequency range compared to the first-order model. The causality of the proposed model is proved and a time-domain representation is derived using the Mittag-Leffler relaxation function.

Comparisons between the proposed model with existing causal models brings insight to the relationships between different causal models developed by independent researchers, leading to the development of a unifying framework of causal RILD models. It is elucidated that the proposed model can include both Makris and Keivan models as its special cases with $\alpha = 0$ and $\alpha = 1$, respectively. It is further illustrated by comparing the proposed model with designed TMW models that the proposed model with a fractional order is equivalent to a TMW model, which is used to approximate Biot model for practical applications. Moreover, Keivan model is shown to be equivalent to a first-order approximation of Biot model.

Lastly, a mechanical representation of the proposed model is developed to physically realize the proposed model in practical engineering applications.

ACKNOWLEDGMENTS

This work was supported by a Grant-in-Aid for Scientific Research (B) (No. 18H01577) provided by the Japan Society for the Promotion of Science (JSPS).

References

1. Ikago K, Inoue N. Behavior of rate-independent linear damping incorporated into long-period structures subjected to strong ground motions. In: Proceedings of the 6th World Conference on Structural Control and Monitoring, Barcelona, Spain. ; 2014: 1116–1124.
2. Luo H, Ikago K, Chong C, Keivan A, Phillips B. Performance of low-frequency structures incorporated with rate-independent linear damping. *Engineering Structures* 2019; 181: 324–335.
3. Scanlan RH, Rosenbaum R. *Introduction to the study of Aircraft Vibration and Flutter*. Dover Publications . 1951.
4. Bishop R. The treatment of damping forces in vibration theory. *Journal of the Royal Aeronautical Society* 1955; 59(539): 738–742.
5. Reid T. Free vibration and hysteretic damping. *The Aeronautical Journal* 1956; 60(544): 283–283.
6. Crandall SH. Dynamic response of systems with structural damping. tech. rep., Massachusetts Institute of Technology, Cambridge, Massachusetts; 1961.
7. Biot MA. Linear thermodynamics and the mechanics of solids. In: Proceedings of the 3rd U.S. National Congress of Applied Mechanics, ASME, New York. ; 1958: 1–18.
8. Caughey T. Vibration of dynamic system with linear hysteretic damping (linear theory). In: Proceedings of 4th U.S. National Congress of Applied Mechanics, ASME, New York. ; 1962: 87–97.
9. Reggio A, De Angelis M, Betti R. A state-space methodology to identify modal and physical parameters of non-viscously damped systems. *Mechanical Systems and Signal Processing* 2013; 41(1-2): 380–395.
10. Makris N. Causal hysteretic element. *Journal of engineering mechanics* 1997; 123(11): 1209–1214.
11. Muscolino G, Palmeri A, Ricciardelli F. Time-domain response of linear hysteretic systems to deterministic and random excitations. *Earthquake engineering and structural dynamics* 2005; 34(9): 1129–1147.
12. Spanos PD, Tsavachidis S. Deterministic and stochastic analyses of a nonlinear system with a Biot visco-elastic element. *Earthquake engineering and structural dynamics* 2001; 30(4): 595–612.
13. Muravskii G. On frequency independent damping. *Journal of Sound and Vibration* 2004; 274(3-5): 653–668.
14. Muravskii G. Linear models with nearly frequency independent complex stiffness leading to causal behaviour in time domain. *Earthquake engineering and structural dynamics* 2007; 36(1): 13–33.
15. Nakamura N. Practical causal hysteretic damping. *Earthquake Engineering and Structural Dynamics* 2007; 36(5): 597–617.
16. Genta G, Amanti N. On the equivalent viscous damping for systems with hysteresis. *Atti della Accademia delle Scienze di Torino* 2009; 32: 21–43.
17. Huang Y, Sturt R, Willford M. A damping model for nonlinear dynamic analysis providing uniform damping over a frequency range. *Computers and Structures* 2019; 212: 101–109.
18. Keivan A, Phillips BM, Ikenaga M, Ikago K. Causal realization of rate-Independent linear damping for the protection of low-Frequency structures. *Journal of Engineering Mechanics* 2017; 143(9): 04017058.

19. Keivan A, Phillips BM, Ikago K. Adaptive causal realization of rate-independent linear damping. *Engineering Structures* 2018; 167: 256–271.

20. Bagley RL, Torvik J. Fractional calculus-a different approach to the analysis of viscoelastically damped structures. *AIAA journal* 1983; 21(5): 741–748.

21. Gaul L, Klein P, Kemple S. Damping description involving fractional operators. *Mechanical Systems and Signal Processing* 1991; 5(2): 81–88.

22. Crandall SH. The role of damping in vibration theory. *Journal of sound and vibration* 1970; 11(1): 3–IN1.

23. Inaudi JA, Kelly JM. Linear hysteretic damping and the Hilbert transform. *Journal of Engineering Mechanics* 1995; 121(5): 626–632.

24. Inaudi JA, Makris N. Time-domain analysis of linear hysteretic damping. *Earthquake Engineering and Structural Dynamics* 1996; 25(6): 529–546.

25. Gradshteyn IS, Ryzhik IM. *Table of integrals, series, and products*. Academic press . 2014.

26. Makris N. Stiffness, flexibility, impedance, mobility, and hidden delta function. *Journal of engineering mechanics* 1997; 123(11): 1202–1208.

27. Lighthill MJ. *An introduction to Fourier analysis and generalised functions*. Cambridge University Press . 1958.

28. Luo H, Chong C, Ikago K, Keivan A, Phillips B. Passive implementation of rate-independent linear damping using a negative stiffness element. In: Proceedings of the 11th U.S. National Conference in Earthquake Engineering, Earthquake Engineering Research Institute, Los Angeles, CA. ; 2018.

29. Luo H, Hanzawa Y, Ikago K. Seismic performance enhancement of a base-isolation structure by using a passive rate-independent damping model. In: Proceedings of the 7th Asia Conference on Earthquake Engineering, Bangkok, Thailand. ; 2018: 1–8.

30. Makris N, Zhang J. Time-domain viscoelastic analysis of earth structures. *Earthquake Engineering and Structural Dynamics* 2000; 29(6): 745–768.

31. Reggio A, De Angelis M. Modelling and identification of structures with rate-independent linear damping. *Meccanica* 2015; 50(3): 617–632.

32. Marple Jr SL. *Digital spectral analysis with applications*. Englewood Cliffs, NJ, Prentice-Hall, Inc. . 1987.

33. Markushevich AI. *Theory of functions of a complex variable*. 296. American Mathematical Society . 2005.

34. Berberan-Santos MN. Properties of the Mittag-Leffler relaxation function. *Journal of Mathematical Chemistry* 2005; 38(4): 629–635.

35. Caputo M, Mainardi F. A new dissipation model based on memory mechanism. *Pure and applied Geophysics* 1971; 91(1): 134–147.

36. Bagley RL, Torvik PJ. On the fractional calculus model of viscoelastic behavior. *Journal of Rheology* 1986; 30(1): 133–155.

37. Samko SG, Kilbas AA, Marichev OI. *Fractional integrals and derivatives: theory and applications*. Gordon and Breach Science . 1993.

38. Sarlis AA, Pasala DTR, Constantinou M, Reinhorn A, Nagarajaiah S, Taylor D. Negative stiffness device for seismic protection of structures. *Journal of Structural Engineering* 2012; 139(7): 1124–1133.

39. Koh CG, Kelly JM. Application of fractional derivatives to seismic analysis of base-isolated models. *Earthquake engineering and structural dynamics* 1990; 19(2): 229–241.

40. Makris N, Constantinou M. Fractional-derivative Maxwell model for viscous dampers. *Journal of Structural Engineering* 1991; 117(9): 2708–2724.

41. Luo H, Ikago K. A generalized model of approximated rate-independent linear damping incorporated into base-isolated structures. In: Proceedings of the 17th World Conference on Earthquake Engineering, Sendai, Japan. ; 2020. Paper No. C001367.

□